Distributed Displacement Response Investigation Technique for Bridge Structures Using Smartphones

Xuefeng Zhao, A.M.ASCE[1]; Qingan Zhao, S.M.ASCE[2]; Yan Yu[3]; Yuting Chen[4]; Hao Liu[5]; Mingchu Li[6]; and Jinping Ou[7]

Abstract: The vertical displacement of a cross section of a bridge has a close correlation with the carrying capacity and the ability to resist dynamic loads. Therefore it has been one of the most important parameters for structural health monitoring and safety assessment. Moreover, when a natural disaster such as a hurricane or an earthquake occurs, a large number of bridges will be affected. To evaluate safety performance and investigate failures preliminarily, rapid inspections of displacement are essential for bridges. This paper presents a bridge distributed displacement investigation technique using smartphones. This smartphone-based technique is a beneficial complement to conventional structural health monitoring techniques for its cost efficiency and operability. Based on photogrammetry technology, an algorithm is used to develop an app called *D-Viewer*. Multipoint dynamic displacement monitoring is implemented synchronously using smartphones. Experiments conducted in the laboratory with reduced-scale models show that this technique is able to monitor the distributed displacement response with reasonable precision. Through data processing, performance of bridges will be evaluated. Low cost and convenience of this technique make it possible for anyone to monitor or inspect the displacement of every short and medium span bridge preliminarily.
DOI: 10.1061/(ASCE)CF.1943-5509.0001025.

Author keywords: Displacement; Bridges; Smartphone; Multipoint; Inspection; Monitoring.

Introduction

Bridges are among the most crucial parts of transportation systems, whose construction and maintenance become an important part of infrastructure development in every country. Under conditions of long-term loading, shrinkage, and creep, and the influence of extreme natural disasters or artificial factors, the structure will suffer different degrees of damage, which can result in accidents, causing huge economic losses (Housner et al. 1997).

Therefore, to ensure the security and durability of bridge structures, structural health monitoring (SHM) for bridges is necessary to detect and prevent failures and prolong their service life. SHM can determine damage to bridge structures and detect security risks as soon as possible, thus ensuring the security of people and property (Brownjohn 2007). Furthermore, when the structure is in a state of emergency or serious anomalies, the SHM system can trigger an alarm and provide guidance for structure repair, maintenance, and management decisions (Balageas et al. 2010). It has become an important means to ensure the security of infrastructure (Ou 2005). However, most SHM systems are designed, integrated, and installed into the infrastructure by professionals and equipped with relatively expensive sensors and data acquisition and transmission facilities, and such systems cannot be installed on every bridge. Hence it is essential to develop more convenient and public-oriented techniques which involve smaller and low-cost devices. These techniques can play a formidable role in SHM, especially in extreme situations such as earthquakes, tornados, floods, and wars, which require rapid failure investigation and security evaluation (Yu et al. 2015).

With the development of modern technology, apps with various advanced functions can be installed on smartphones. By the end of 2015, there were approximately 1.86 billion smartphone users worldwide according to Statista (2016). These smartphones, with their cost-effective infrastructure, contribute more than 90 percent of data connections in the world (Ozcan 2014). Using built-in smartphone functions such as the camera, accelerometer, gyroscope, and GPS, it is possible to combine smartphone technology with SHM. If it is implemented successfully, the ability to monitor and quickly inspect every structure during certain emergencies will eventually come true. Furthermore, smartphones are capable of sending collected monitoring data to a server so that large-scale SHM can be realized (Zhao et al. 2015c). Smartphones are used as sensor data receiving and analysis devices, and thus could realize public participation in SHM (Yu et al. 2012; Yi et al. 2012, 2013). Currently, a few preliminary studies have used the built-in functions of smartphones to determine some SHM parameters

[1]Professor, State Key Laboratory of Coastal and Offshore Engineering, School of Civil Engineering, Dalian Univ. of Technology, No. 2 Linggong Rd., Dalian 116024, China (corresponding author). E-mail: zhaoxf@dlut.edu.cn

[2]Undergraduate Student, State Key Laboratory of Coastal and Offshore Engineering, School of Civil Engineering, Dalian Univ. of Technology, No. 2 Linggong Rd., Dalian 116024, China.

[3]Professor, School of Electronic Science and Technique, Dalian Univ. of Technology, No. 2 Linggong Rd., Dalian 116024, China.

[4]Undergraduate Student, State Key Laboratory of Coastal and Offshore Engineering, School of Civil Engineering, Dalian Univ. of Technology, No. 2 Linggong Rd., Dalian 116024, China.

[5]Graduate Student, State Key Laboratory of Coastal and Offshore Engineering, School of Civil Engineering, Dalian Univ. of Technology, No. 2 Linggong Rd., Dalian 116024, China.

[6]Professor, School of Software Technology, Dalian Univ. of Technology, No. 2 Linggong Rd., Dalian 116024, China.

[7]Professor, State Key Laboratory of Coastal and Offshore Engineering, School of Civil Engineering, Dalian Univ. of Technology, No. 2 Linggong Rd., Dalian 116024, China; School of Civil Engineering, Harbin Institute of Technology, No. 92 West Dazhi St., Harbin 150001, China.

Note. This manuscript was submitted on June 8, 2016; approved on December 6, 2016; published online on February 27, 2017. Discussion period open until July 27, 2017; separate discussions must be submitted for individual papers. This paper is part of the ***Journal of Performance of Constructed Facilities***, © ASCE, ISSN 0887-3828.

(Zhao et al. 2016; Oraczewski et al. 2016; Ozer et al. 2015; Feng et al. 2015; Höpfner et al. 2013). In 2013, an app called *iShake* was developed which enabled smartphones to be used as seismic sensors (Reilly et al. 2013). In 2014, an app called *Orion CC* was developed for cable force monitoring of suspension bridges (Zhao et al. 2015b).

Photogrammetry is an advanced noncontact measurement method which has massive far-reaching prospects. Sangho (2001) developed a structure displacement monitoring software system based on close-range photogrammetry technology (CRP), and a corresponding experiment was implemented on a suspension bridge model. Mazen et al. (2003) measured the deformation of the Vincent Thomas Bridge in California based on photogrammetry. They arranged a fixed reference point and a point to be measured and used a camera shooting a black steel plate with a red light emitting diode (LED) lamp to obtain the displacement of the bridge. Lee and Shinozuka (2006) also used a camera shooting a mark with a known shape to obtain displacement. This method was then applied to a steel-plate girder bridge. After comparing the photographs with the results of the displacement sensors, they obtained feasible conclusions. Iwao et al. (2010) integrated LED technology with position sensors and obtained displacement–time curves with the help of photosensitive technology.

Displacement is directly related to the strain on a point and is a basic reflection of the dynamic effects, which can be used for evaluating safety performance and investigating failures (Kwasniewski et al. 2006). It can also be used to prevent failures such as the buckling of a bridge by determining geometric out-of-plane imperfections (Backer et al. 2014). Furthermore, Zhao et al. (2015a) proposed a displacement sensing technique using video cameras. However, video cameras are still not convenient or efficient enough for quick SHM or inspection. Therefore this paper develops *D-Viewer*, an app for the iPhone operating system (iOS), for distributed displacement response investigation. Recent research shows that displacement of only a few points is enough for damage detection on a bridge, which makes this technique more convenient (Wang et al. 2012). Using the built-in camera of a smartphone, multipoint synchronous monitoring of distributed displacement response is realized.

D-Viewer

Basic Principle

Light intensity and color are the quantitative characteristics of a two-dimensional image, which can be expressed with a two-dimensional function

$$F(x, y) = G(x, y) \cdot H(x, y) \tag{1}$$

where x and y = plane coordinates; G = incidence function, which depends on the energy of incident light amid the light source, reflecting the environmental factors of an image; and H = reflection function, which depends on the reflection characteristics of the surface, reflecting the intrinsic characteristics of an image. G and H together reflect the internal and external factors of an image.

Due to the discrete characteristic of computers, the continuous light intensity of an image must be discretized. Using the imaging device, the light intensity function is divided into $M \times N$ small regions; each cell domain is called a pixel. Several types of partitioning approaches are taken, among which the square grid is the most common method, as shown in Fig. 1.

Meanwhile, it is necessary to quantify the gray value of each pixel. Taking as an example uniform quantization, which is considered the most common method, the gray level of the image is divided into N levels—in other words, the resolution of the image. N is generally 2 to the power of 8, 10, or 16, which corresponds to 256, 1,024, or 65,536 gray levels, respectively.

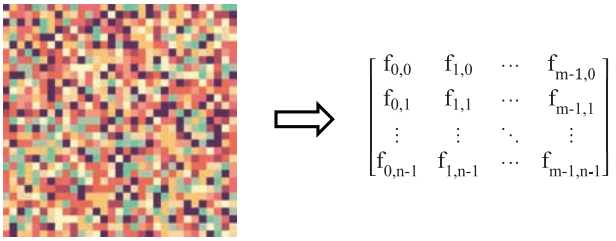

Fig. 1. (Color) Matrix representation of a digital image

The discrete image can then be expressed by a matrix, in which the position of each element corresponds to the plane position of the pixel and the value of each element corresponds to the gray value of the pixel point. Therefore a change in the digital image can be expressed and operated by the matrix. The connection between actual displacement and the image is established.

The displacement monitoring and inspection method implemented on *D-Viewer* is based on displacement monitoring of a laser spot. A laser is fixed on the object to be measured and emits a laser point onto a stationary projection plate. *D-Viewer* is capable of shooting the trajectory of the laser point on the projection board, so the value of displacement of the object to be measured is obtained by movement analysis of the laser point on the projection plate. The method can also be implemented by fixing the projection plate and the smartphone app *D-Viewer* on the object to be measured. The laser is kept motionless, so the value of displacement of the object to be measured can also be obtained by movement analysis of the laser point on the projection board.

Before implementing measurement, *D-Viewer* must determine the relationship between pixel movement and actual displacement, which is achieved by calibration using white paper with a black circle whose diameter is known. To ensure measurement precision, the smartphone and the calibration object must remain relatively stationary during the calibration process, and the background of the black circle must be entirely white. Via calibration, *D-Viewer* can obtain the conversion formula between the pixel movement and the actual displacement, which enables it to obtain the actual displacement value.

The specific steps of *D-Viewer* internal processing are as follows:

1. Calibration
   - *a.* The actual diameter of the black circle is obtained by information that the user inputs (D).
   - *b.* Binary processing (0, 255) is implemented using *OpenCV*.
   - *c.* The maximum width of the black pixels within the range of the camera is obtained (L).
   - *d.* The ratio of the two is calculated: Ratio = D/L.
2. Measurement
   - *a.* The pixel positions of the monitoring region are obtained according to the information input by the user.
   - *b.* The coordinates of all pixels whose value is 0 are obtained. (Compared with the background, the laser point is much brighter, so when the binary processing is complete, the pixel value of the laser point should be 0, whereas the pixel value of the background should be 255.) The average horizontal and vertical coordinates (x, y) are obtained and are equivalent to the centroid coordinates of the laser spot. The calculation method of the average value is to sum up all values of

horizontal and vertical coordinates; the results are SUMX and SUMY, respectively. The centroid coordinate is determined by (SUMX/N, SUMY/N), where N is the total number of pixels.

c. The centroid pixel coordinate is converted to the coordinates of the actual position

$$x_1 = x \cdot \text{Ratio} \tag{2}$$

$$y_1 = y \cdot \text{Ratio} \tag{3}$$

d. The first frame is considered as the initial point, so the instantaneous displacement (Δx_1, Δy_1) is obtained when (x_1, y_1) is compared with the previous frame.

Operation Guide

To begin, the *D-Viewer* app is opened on the smartphone. The initial settings interface appears as shown in Fig. 2. The diameter of the calibration object (black circle) in millimeters is input into the first line of the upper-right corner; the front or rear camera is selected in the second line; the monitoring area (length and width, in millimeters) is input into the third line; and the lines of the pixel scanning interval are input into the fourth line. (Sometimes it is unnecessary to scan all pixels, so this fourth line is optional, and the default value is 0.)

The smartphone and the projection plate are secured in parallel, and both should be kept relatively stationary until the end of monitoring. The calibration object is placed on the projection plate, as shown in Fig. 3.

The calibration interface appears when the initial settings are complete, as shown in Fig. 4. To separate the calibration object from the background clearly, Button A is used to adjust the threshold of the calibration interface. The Ratio button in the interface executes a program that automatically calculates the ratio of actual displacement and pixel displacement.

Next, an interface allows the user to choose whether to monitor the displacement of the calibration object directly or to monitor laser spot displacement, as shown in Fig. 5. In this example, the latter is chosen.

The calibration object is removed and the laser is activated to irradiate the projection plate. The Switch button launches the scope adjustment interface as shown in Fig. 6. The four buttons in the lower-left corner of the screen are used to adjust the scope of the monitoring area in order to cover all regions in which the laser point will move. Once this is done, Button B adjusts the threshold of the interface so that the laser spot can be separated from the background clearly, as shown in Fig. 6. Other parts of the camera view shall be entirely black. Tapping the Start button begins the monitoring of the centroid coordinates of the laser spot, as shown in Fig. 7.

In the process of monitoring, *D-Viewer* sets the position of the laser point in the first frame of the video signals as the origin of coordinates. After processing video signals, *D-Viewer* can obtain the centroid pixel coordinate of the laser point in each frame and calculate the value of the actual coordinate. All of these are

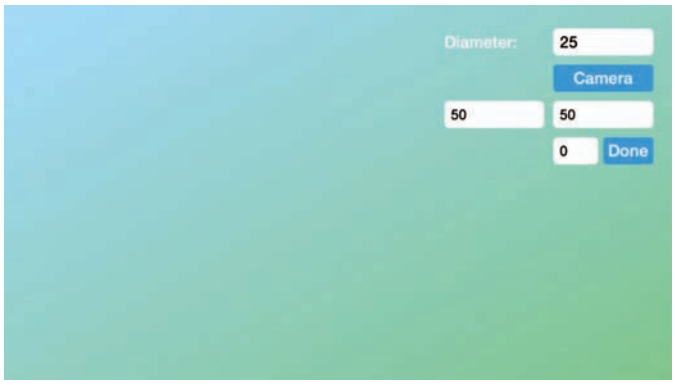

Fig. 2. (Color) Initial settings interface

Fig. 3. (Color) Schematic diagram of the devices

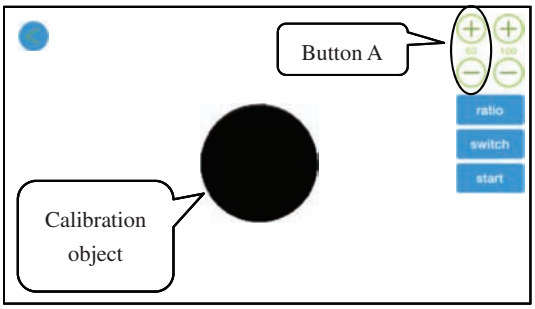

Fig. 4. (Color) Calibration interface

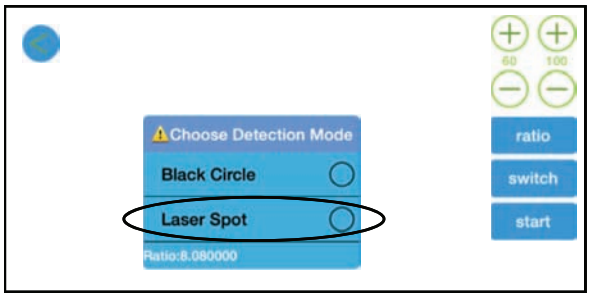

Fig. 5. (Color) Interface of selecting a monitoring method

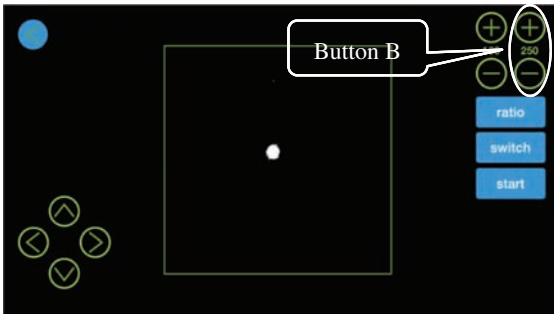

Fig. 6. (Color) Scope adjustment interface

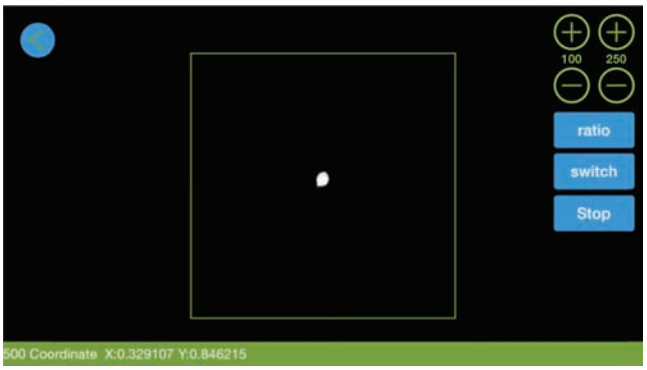

Fig. 7. (Color) Monitoring interface

processed in real time, so the displacement of the object to be monitored is manifested directly.

The actual centroid coordinate of the laser point is displayed on the bottom of the interface in real time. The Stop button terminates monitoring, and data in .txt format are stored in the root directory of the app.

Experiment and Results

To verify the feasibility of the new method in this paper, a series of static and dynamic displacement experiments was carried out. The static part included a simple loading experiment, involving determination of the overall deformation curves of a suspension bridge model under the condition of loading on the mid span and the displacement influence line of the mid span. These sets of experiments were implemented to verify the stability of the new method under the condition of slow loading, which simulates the static displacement monitoring or inspection in practical engineering. The dynamic part included displacement monitoring of a shaking table and determination of the overall deformation graph of a suspension bridge model in real time under impact loading on the mid span. These sets of experiments were implemented to ensure that this new method is capable of capturing the real-time displacement that changes at a rapid pace, which simulates dynamic displacement monitoring or inspection in practical engineering. Furthermore, all results of the experiment were compared with the laser displacement sensor and dial indicators to verify the precision of the new method.

Because sampling frequency is one of the important parameters for displacement monitoring, data acquisition tests were implemented using iPhone 6 and iPhone 6 Plus. Results of the tests for a stable rate are obtained, as shown in Fig. 8. The six columns from left to right represent the test date, hour, minute, second, X coordinate and Y coordinate. The number of data points acquired per second for both iPhone 6 and iPhone 6 Plus was 30, which indicates that the sampling frequency of both the iPhone 6 and iPhone 6 Plus is 30 Hz. Also, tests showed that the data collection interval was stable in the process. Related parameters are shown in Table 1 (Apple 2016), from which it can be seen that iPhone 6 and iPhone 6 Plus have the same chip and video recording features, indicating that their precision is the same.

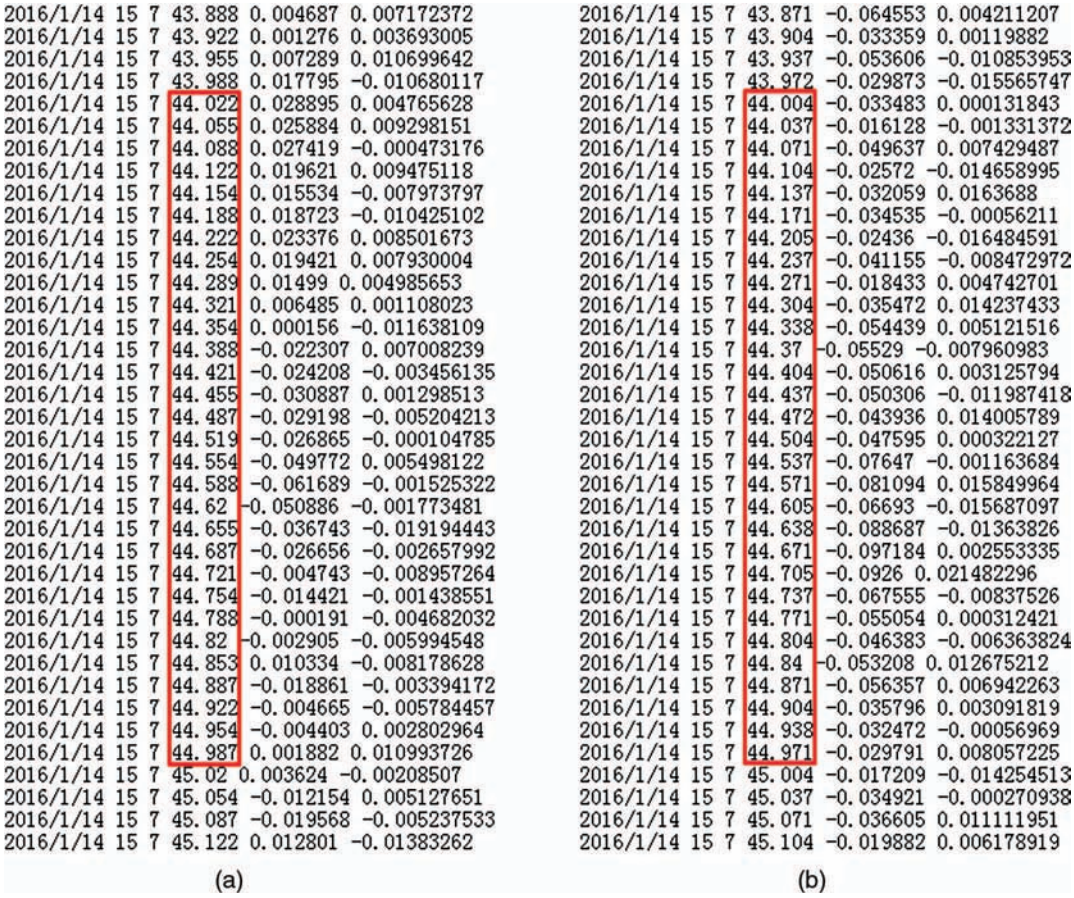

Fig. 8. (Color) (a) Results of data acquisition test (iPhone 6); (b) results of data acquisition test (iPhone 6 Plus)

Table 1. Parameters of iPhone 6 and iPhone 6 Plus

Model	Operating system	Display	Chips	Video recording	Sensors
iPhone 6	iOS 8.4.1	Retina high definition (HD) display 4.7-in (diagonal) 1,334-by-750-pixel resolution at 326 pixels per in. (PPI) 1,400:1 contrast ratio (typical)	A8 chip with 64-bit architecture M8 motion coprocessor	1,080p HD video recording	Barometer Three-axis gyro Accelerometer Proximity sensor Ambient light sensor
iPhone 6 Plus	iOS 8.4.1	Retina HD display 5.5-in (diagonal) 1,920-by-1,080-pixel resolution at 401 PPI 1,300:1 contrast ratio (typical)	A8 chip with 64-bit architecture M8 motion coprocessor	1080p HD video recording	Barometer Three-axis gyro Accelerometer Proximity sensor Ambient light sensor

Simple Loading Experiment

Experiment Description

The simple loading-displacement experiment was carried out to verify the precision of the new displacement monitoring and inspection method under the condition of static displacement. Experimental apparatuses included an iPhone 6 Plus, a displacement loading device, a laser transmitter, a black projection plate with angle scale, A4 paper with calibration objects, a laser displacement sensor, and a computer.

The displacement loading device was composed of a base and a moving part, which was capable of moving along the base. The displacement was controlled by rotating the knob on the device, which resulted in displacement of 0.35 mm per rotation. Because of the low loading speed, the process can be regarded as static. The laser transmitter was fixed on the moving part and the sensor connected with a computer was fixed on the base to monitor the displacement of the laser transmitter accurately. The iPhone 6 Plus was fixed directly in front of the projection plate when initialization was complete. The camera of the iPhone 6 Plus and the projection plate were kept parallel and relatively static until the conclusion of the experiment. The laser transmitter was adjusted so that it produced a bright spot on the projection board. If the projection board is vertical to the direction of the laser light, the smartphone is likely to block the beam, which compromises the displacement monitoring. Therefore the projection plate and the direction of the beam were set at an angle of 30° using the angle scale on the projection plate. By geometric relationship, the displacement measured is twice the actual value. Thus data from the iPhone 6 Plus must be divided by 2. It should be noted that ensuring the precise installation angle may be difficult, and a potential angle change of the projection plates due to rotation of the structure at the installation location may cause errors in field use. However, these limits are likely to be overcome by a displacement error back-propagation method using multiple laser transmitters (Jeon et al. 2012). The schematic diagram and photo are shown in Fig. 9.

D-Viewer was calibrated using the Operation Guide presented previously. The laser transmitter was turned on when the calibration was complete, and the sensor and *D-Viewer* were activated simultaneously. The knob was rotated slowly so that the laser transmitter and the laser point on the projection plate generated the same displacement. Therefore the displacement was obtained by both the sensor and *D-Viewer*, whose data needed to be divided by 2. Two sets of experiments were implemented as follows.

Experiment A: The knob was rotated to allow the laser transmitter to move away from the sensor slowly. After movement of approximately 4.7 mm, the knob was reversed to move the laser transmitter closer to the sensor until the laser transmitter had returned to its original position. Data were then collected.

Experiment B: Because of experimental errors, displacement measured by the sensor is not entirely accurate. To compare the experimental data with actual displacement, the following approach

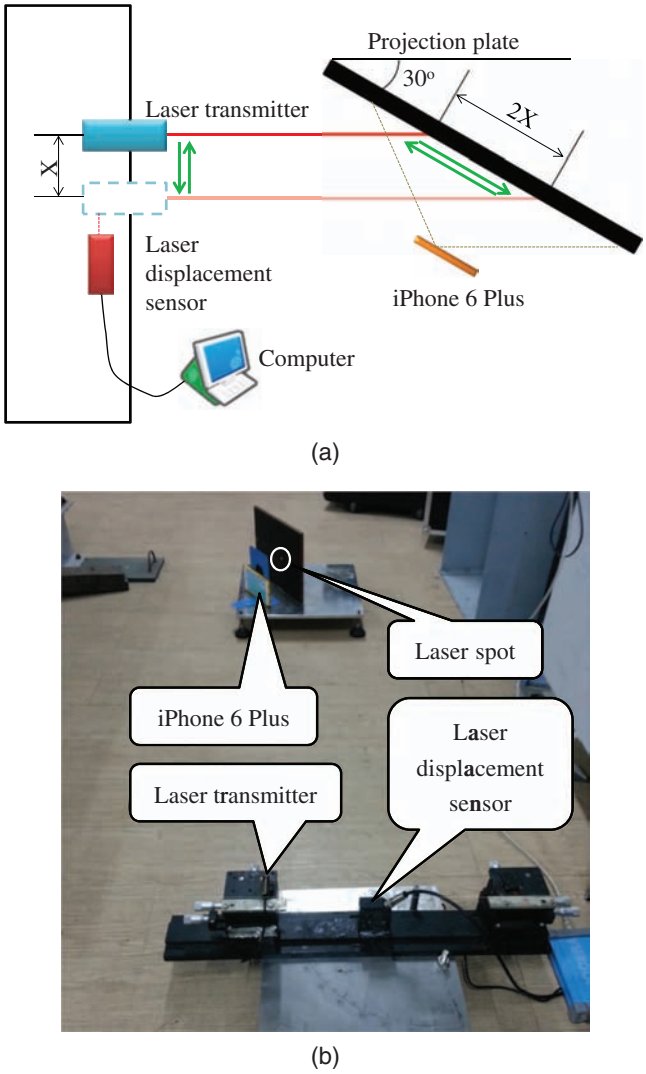

Fig. 9. (Color) (a) Schematic diagram of the simple loading experiment; (b) photo of the simple loading experiment

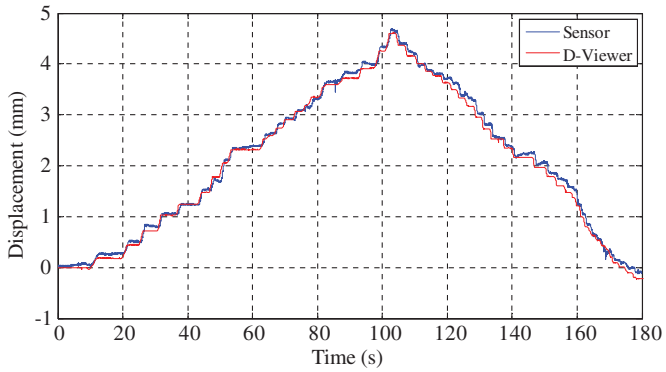

Fig. 10. (Color) Result of sensor and *D-Viewer* in simple loading Experiment A

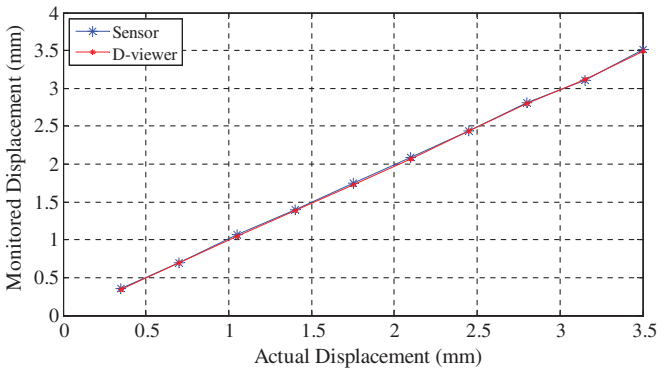

Fig. 11. (Color) Result of simple loading Experiment B

was taken: data were recorded and processed for each full turn of the knob. The total number of turns was 10, so the value of actual displacement was $0.35\ \text{mm} \times 10 = 3.5\ \text{mm}$. Finally, the results from the sensor and *D-Viewer* were compared with the actual displacement.

Experiment Results

Experiment A: Displacement–time curves obtained by the sensor and *D*-Viewer are shown in Fig. 10. The two displacement–time curves fit well. Although there are a few errors, all of them are within an acceptable level, and *D-Viewer* was more stable than the sensor according to the result. The peak value of *D-Viewer* was 4.612 mm, whereas it was 4.692 mm for the sensor, an error of only 1.71%.

Experiment B: Displacement of each turn was monitored by the sensor and *D-Viewer*, as shown in Table 2 and Fig. 11.

The error rate between the displacement measured by *D-Viewer* and the true value was within 3%. Therefore it can be concluded that *D-Viewer*'s accuracy is high in terms of micro displacements.

Static Experiment with Bridge Model

Experiment Description

Because the displacement monitoring and inspection method of this paper is mainly for bridge engineering, *D-Viewer* should be capable of accurately measuring the deformation of the bridge under the condition of static loading.

A concrete self-anchored suspension bridge model was adopted in the experiment. The prototype of the bridge is located in Zhuanghe City, China, with a span arrangement of $70 + 200 + 70 = 340$ m, a deck width of 27 m, and a box girder of reinforced concrete. The model was built at a 1:28 scale, with a span arrangement of $2.5 + 7.14 + 2.5 = 12.14$ m; the beam was solid concrete, and the main cables and hangers were wire rope.

Table 2. Result of simple loading Experiment B

Loop	Actual value (mm)	*D-Viewer* (mm)	Sensor (mm)	Error of *D-Viewer* (mm) (%)	Error of the sensor (%)
1	0.35	0.341	0.36	2.57	2.86
2	0.7	0.701	0.693	0.14	1.00
3	1.05	1.043	1.068	0.67	1.71
4	1.4	1.385	1.395	1.07	0.36
5	1.75	1.722	1.748	1.60	0.11
6	2.1	2.066	2.09	1.62	0.48
7	2.45	2.438	2.44	0.49	0.41
8	2.8	2.799	2.808	0.04	0.29
9	3.15	3.122	3.105	0.89	1.43
10	3.5	3.488	3.517	0.34	0.49

According to the theory of similitude (Fumagalli 1973), the following equation can be drawn:

$$S_D = S_F \cdot S_L^3 \cdot S_E^{-1} \cdot S_I^{-1} \tag{4}$$

where S_D = displacement ratio of the model to the actual bridge; S_F = concentrated load ratio; S_L = length ratio; S_E = elastic modulus ratio; and S_I = moment of inertia ratio. According to the model, $S_L = 28$, $S_E = 1$, and $S_I = S_L$ to the 4th power. Therefore in the experiment S_D was set equal to 1 and S_F had to be the reciprocal of S_L, which was $1/28$, so weights of $1/28$ the mass of normal cars were used to generate the actual displacement.

Experimental apparatuses included an iPhone 6 Plus, four iPhone 6's, five laser transmitters, several loading weights, a trolley, five black projection plates with angle scale, five dial indicators, and A4 paper with calibration objects. Two sets of experiment were implemented as follows.

Experiment A: This experiment was implemented to determine the deformation curves of the model under the condition of loading on the mid span. Five measuring points spaced 1.07 m apart were set, of which Point 3 was exactly on the mid span. The projection plates and smartphones were fixed on the five measuring points, of which Point 3 was monitored by the iPhone 6 Plus and the rest were monitored by iPhone 6's. Laser transmitters were set on both sides of the model. There were three laser transmitters on one side and two on the other, each of which corresponded to a projection plate on the measuring point. All laser transmitters remained stationary during the whole process, and when displacement occurred at a measuring point the projection plate and smartphone moved the same distance. Because the laser transmitters were static, the laser spot on the projection plate also moved the same distance but in an opposite direction. Therefore the displacement monitored by *D-Viewer* took the opposite number. Meanwhile, dial indicators were set beneath the model at corresponding measuring points to verify the precision of displacement monitoring by *D-Viewer*.

Step loading was employed in this experiment using 18-kg weights. To eliminate the condition in which the deformation of both sides of the deck is asymmetric, a weight was loaded on each side of the deck in every step. The experiment was implemented with a process of loading–loading–unloading–unloading. There were intervals between each two steps to ensure the stability of the deformation. The schematic diagram and photos are shown in Fig. 12.

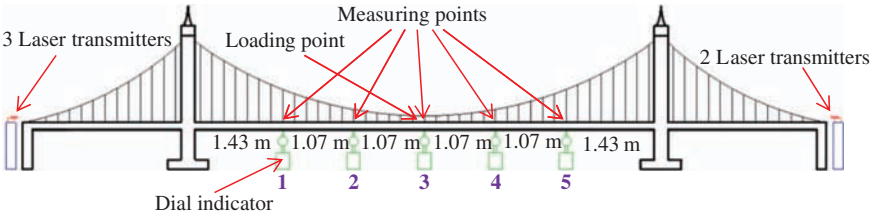

(a)

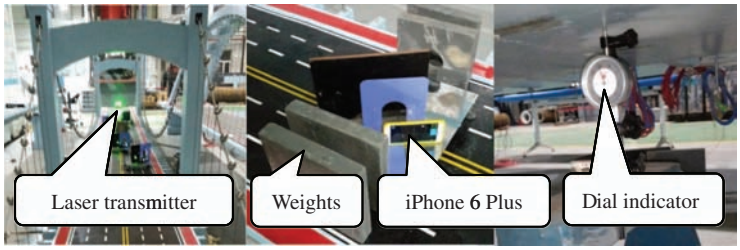

(b)

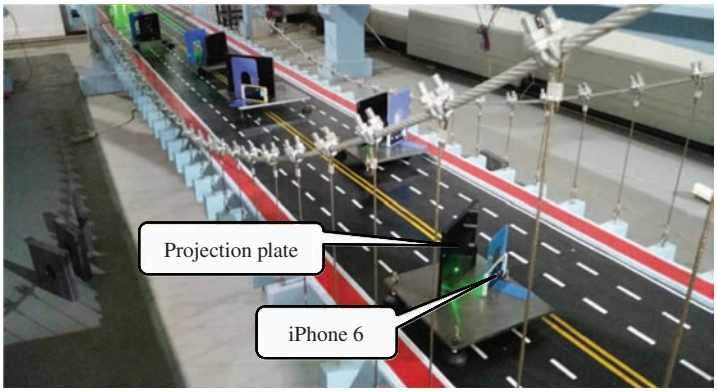

(c)

Fig. 12. (Color) (a) Schematic diagram of static bridge Experiment A; (b) photos of static bridge Experiment A; (c) photo of static bridge Experiment A

Experiment B: This experiment was implemented to determine the displacement influence line of the mid span. There was only one measuring point set on the mid span whose arrangement mode was exactly the same as Experiment A. Because of the symmetry, measuring half the model was enough. To begin, a trolley with a weight of 60 kg was set on the deck over the right pier. It was moved slowly toward the mid span, and both *D-Viewer* and the dial indicator data were recorded every 17 cm (a total of 20 records). The schematic diagram and photo are shown in Fig. 13.

Experimental Results

Experiment A: The results are shown in Table 3 and Fig. 14.

As seen in Table 3, the maximum error rate was 6.15% but otherwise did not exceed 5%. Meanwhile, from the viewpoint of the displacement–time curve obtained via *D-Viewer*, the synchronization was good and the data were stable. Therefore deformation curves of the model and displacement variation of each point were obtained, as shown in Figs. 15 and 16.

Both Figs. 15 and 16 can be used to analyze the performance of the structure. Normally, deformation curves should be symmetric when loading on the mid span. If one or more parts are damaged, the stiffness of such parts will change, which may cause asymmetry of the deformation curve. Also, displacement variation of each point is approximately linear under normal conditions. Damage

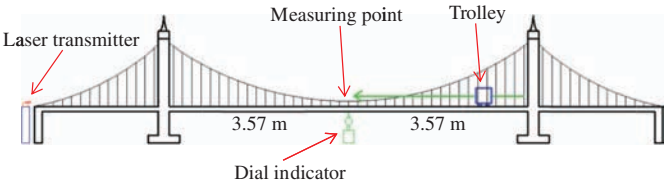

(a)

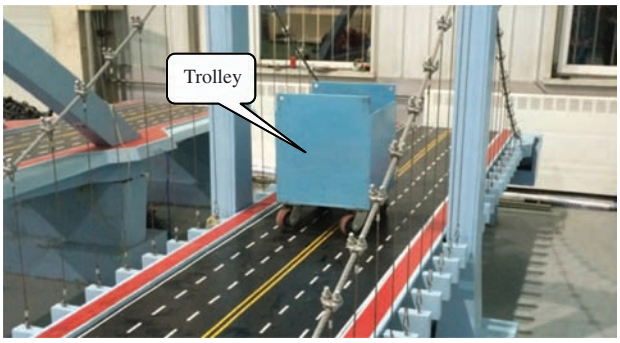

(b)

Fig. 13. (Color) (a) Schematic diagram of static bridge Experiment B; (b) photo of static bridge Experiment B

Table 3. Data Comparison of *D-Viewer* and the Dial Indicators in Static Bridge Experiment A

Point	Status	Initial	First loading	Second loading	First unloading	Second unloading
Point 1	*D-Viewer* (mm)	0	0.237	0.396	0.259	0.010
	Dial indicator (mm)	0	0.232	0.380	0.250	0.010
	Error (%)	—	2.16	4.21	3.60	0
Point 2	*D-Viewer* (mm)	0	0.536	1.070	0.596	0.046
	Dial indicator (mm)	0	0.515	1.040	0.580	0.045
	Error (%)	—	4.08	2.88	2.76	2.22
Point 3	*D-Viewer* (mm)	0	0.739	1.486	0.850	0.069
	Dial indicator (mm)	0	0.715	1.440	0.815	0.065
	Error (%)	—	3.36	3.28	4.29	6.15
Point 4	*D-Viewer* (mm)	0	0.506	1.026	0.578	0.057
	Dial indicator (mm)	0	0.500	1.010	0.560	0.055
	Error (%)	—	1.20	1.58	3.21	3.63
Point 5	*D-Viewer* (mm)	0	0.229	0.455	0.244	0.031
	Dial indicator (mm)	0	0.220	0.440	0.240	0.030
	Error (%)	—	4.09	3.41	1.67	3.33

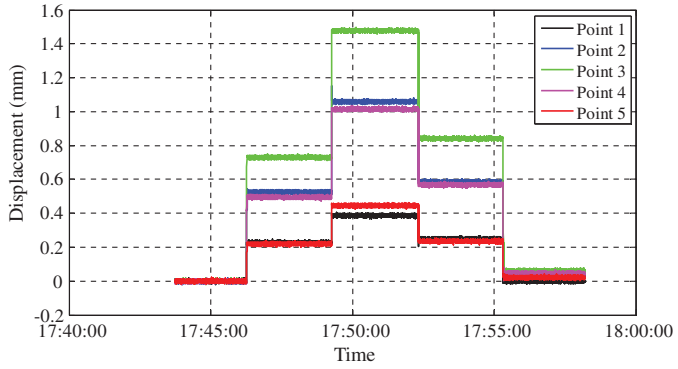

Fig. 14. (Color) Result of all measuring points by *D-Viewer* in static bridge Experiment A

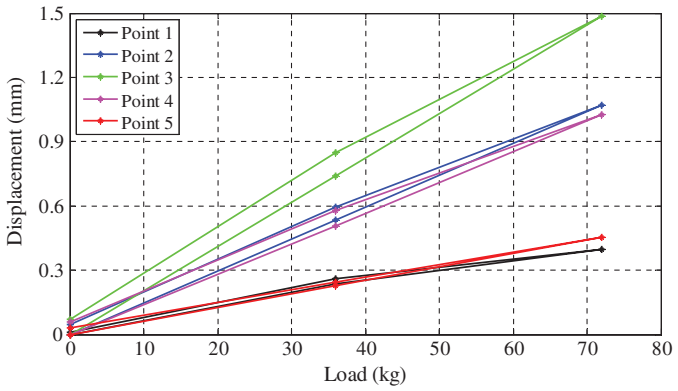

Fig. 16. (Color) Displacement variation of each point

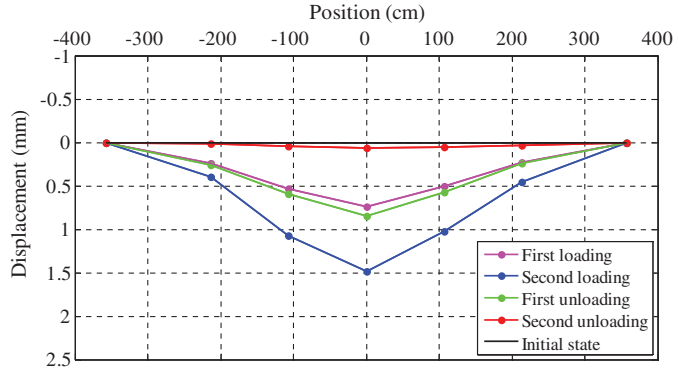

Fig. 15. (Color) Deformation curves of the model

could be detected if some points show an obvious nonlinear change. Moreover, after a sufficient amount of time following unloading, whether or not displacement is reduced to 0 can be used to evaluate the bridge performance as well. The change of local stiffness caused by damage can even be obtained by analyzing displacement of two symmetrical points, according to Wang et al. (2012).

Experiment B: Taking the right pier as the coordinate origin, the displacement of each point was obtained by *D-Viewer* and the dial indicator, as shown in Table 4. Therefore two displacement influence lines of the mid span were obtained, as shown in Fig. 17. The two displacement influence lines fit well, and the maximum error rate was only 3.12%. Thus, in terms of static displacement, the precision and feasibility of the new displacement monitoring and inspection method in this paper were verified.

Because many properties of the displacement influence line—for example, the first derivative—can be obtained under normal conditions, it is possible to detect anomalies in those properties and use those properties for performance evaluation. More research needs to be conducted.

Dynamic Experiment with Vibration Table

Experiment Description

To verify the precision of the new displacement monitoring and inspection method in dynamic conditions, a series of dynamic experiments on a vibration table was implemented. Experimental apparatuses included an iPhone 6 Plus, a vibration table, a computer, a projection plate with angle scale, a laser transmitter, a laser displacement sensor, and A4 paper with calibration objects.

The laser transmitter was fixed on the vibration table to ensure that they had the same displacement when the vibration table was moving. The arrangement of the iPhone 6 Plus and the projection plate was exactly the same as in the simple loading experiment. Displacement of the laser transmitter was obtained by monitoring the laser spot on the projection plate by *D-Viewer*. Meanwhile, a laser displacement sensor, which remained stationary during the whole process, was set next to the vibration table to verify the

Table 4. Data Comparison of *D-Viewer* and the Dial Indicators in Static Bridge Experiment B

Position (cm)	*D-Viewer* (mm)	Dial indicator (mm)	Error (%)
0	0	0	—
17	0.0999	0.10	0.09
34	0.1988	0.20	0.6
51	0.2965	0.30	0.37
68	0.3913	0.39	0.8
85	0.4800	0.49	1.89
102	0.5804	0.58	0.16
119	0.6586	0.67	1.77
136	0.7411	0.76	1.96
153	0.8234	0.84	1.65
170	0.8976	0.91	1.79
187	0.9691	0.99	1.66
204	1.0248	1.05	2.52
221	1.0773	1.11	3.03
238	1.1319	1.16	2.75
255	1.1729	1.21	3.04
272	1.2087	1.25	3.12
289	1.2397	1.28	2.95
306	1.2591	1.30	3.02
323	1.2723	1.31	2.88

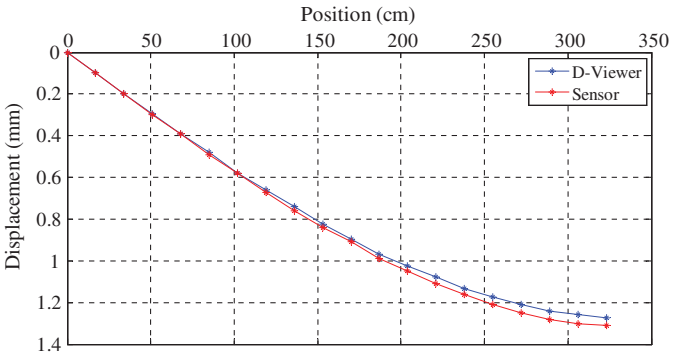

Fig. 17. (Color) Displacement influence lines of mid span

precision of *D-Viewer*. Two sets of experiments were implemented, and the schematic diagram and photos are shown in Fig. 18.

Experiment A: A sine wave with amplitude of 7 mm and frequency of 2 Hz was employed in this experiment.

Experiment B: A simulated seismic wave (Kobe wave) was employed in this experiment.

Experiment Results

Experiment A: The results of the sine wave are shown in Fig. 19 and Table 5.

Experiment B: The results of the Kobe wave are shown in Fig. 20 and Table 6.

As seen in the results, the two series of displacement–time curves fit well, and the data were stable. Several points were chosen to compare, and the error rate was within 5%. Therefore, in terms of dynamic displacement, the precision and feasibility of the new displacement monitoring and inspection method in this paper were verified.

Dynamic Experiment with Bridge Model

Experiment Description

The purpose of this experiment was to simulate the dynamic displacement monitoring of the bridge. *D-Viewer* was used to

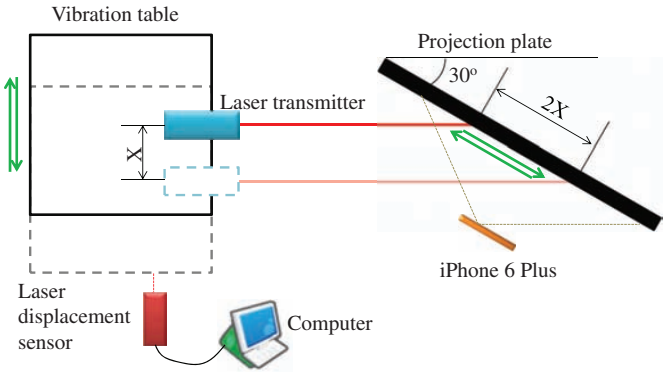

(a)

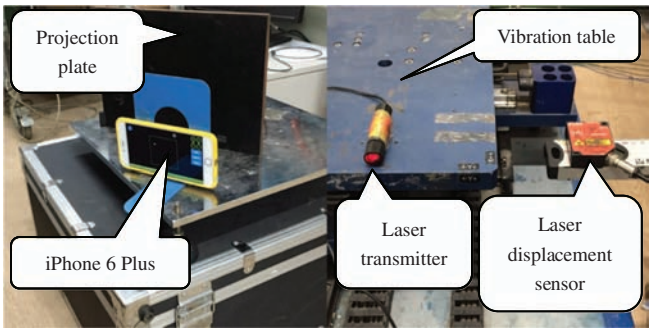

(b)

Fig. 18. (Color) (a) Schematic diagram of dynamic vibration table Experiments A and B; (b) photos of dynamic vibration table Experiments A and B

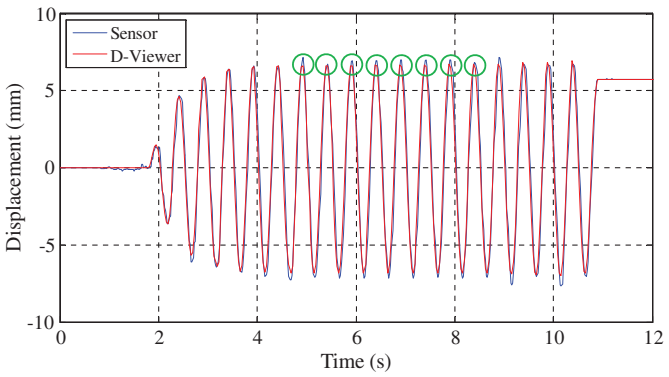

Fig. 19. (Color) Result of both the sensor and *D-Viewer* in dynamic vibration table Experiment A

Table 5. Data Comparison of *D-Viewer* and the Sensor in Dynamic Vibration Table Experiment A

D-Viewer (mm)	Sensor (mm)	Error (%)
6.683	7.018	4.77
6.62	6.613	0.11
6.634	6.920	4.13
6.679	6.957	4.00
6.687	6.690	0.04
6.692	7.013	4.58
6.697	7.002	4.36
6.698	6.850	2.22

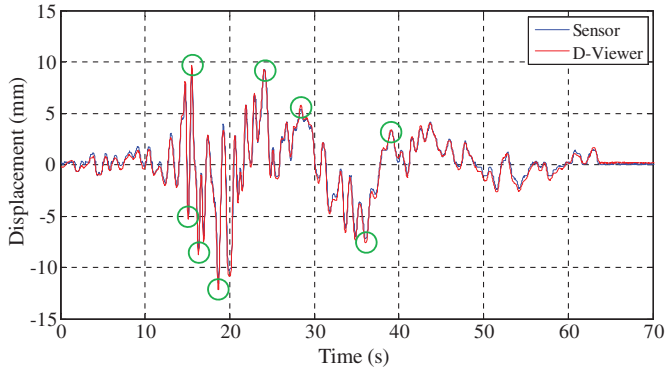

Fig. 20. (Color) Result of both the sensor and *D-Viewer* in dynamic vibration table Experiment B

Table 6. Data Comparison of *D-Viewer* and the Sensor in Dynamic Vibration Table Experiment B

D-Viewer (mm)	Sensor (mm)	Error (%)
9.697	9.415	3.00
−5.296	−5.086	4.13
−8.662	−8.384	3.32
−12.170	−11.680	4.20
9.281	9.262	0.21
5.603	5.483	2.19
−7.592	−7.255	4.65
3.406	3.342	1.92

determine the overall deformation of a bridge model in real time under impact loading on the mid span. The model in this experiment was the same as in the static experiment. Experimental apparatuses included an iPhone 6 Plus, four iPhone 6's, five laser transmitters, a weight for impact, five black projection plates with angle scale, a laser displacement sensor, and A4 paper with calibration objects.

The arrangement of measuring points, laser transmitters, smartphones, and projection plates was exactly the same as in the static experiment. Dial indicators were not used because they cannot capture the real-time displacement. Displacement sensors were arranged above mid span to monitor Point 3 and draw a comparison with *D-Viewer*.

A weight of 18 kg was used to impact the model near Point 3. The schematic diagram and photo are shown in Fig. 21.

Experiment Results

The results are shown in Fig. 22. The synchronization of all measuring points was good. The real-time deformation graph was obtained, as shown in Fig. 23. However, because the impact point was too close to Point 3, the apparatus was negatively affected by the impact, which caused instability of the data in the first second, as shown in Fig. 22(a). More research therefore should be carried out, and *D-Viewer* will be updated to work on this instability issue. Fortunately, smartphone cameras continue to develop. *D-Viewer* will utilize advantages of higher frames per second (FPS) and faster central processing units (CPUs) of smartphones.

To fully evaluate bridge performance, more parameters should be considered. A smartphone has been used to detect acceleration for girder hoisting monitoring (Han et al. 2016). This technique can be used on bridge structures as well. By collecting the vibration signal of displacement and acceleration, the vibration mode, natural frequency, and damping ratio of the bridge can be obtained by spectral analysis. All these parameters can contribute to a more comprehensive evaluation for bridge performance.

Discussion of Real Structures Application

Because the goal is to provide a convenient and efficient preliminary displacement monitoring technique for bridge performance and safety evaluation, it is necessary to discuss how this technique

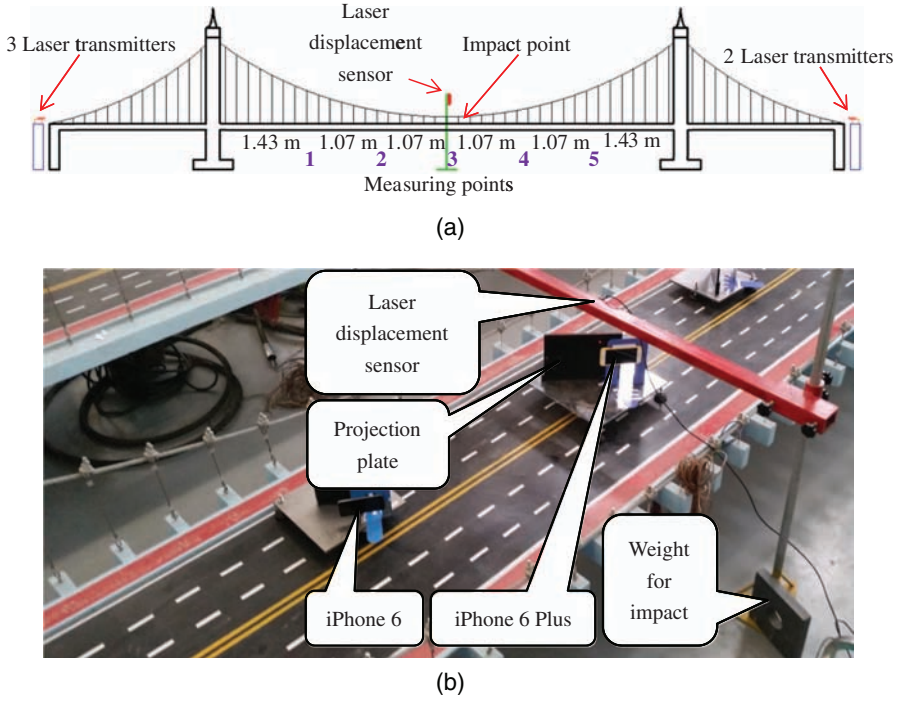

Fig. 21. (Color) (a) Schematic diagram of dynamic bridge experiment; (b) photo of the experiment

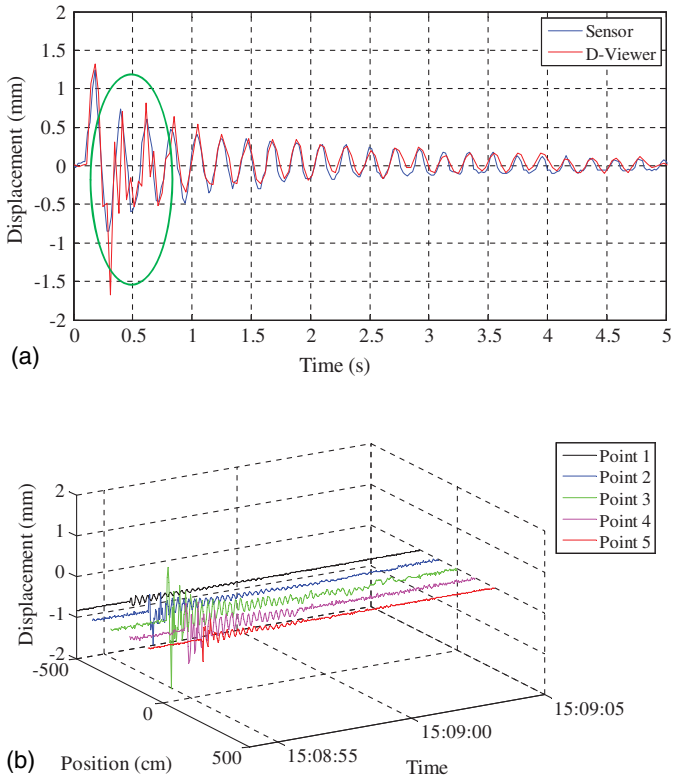

Fig. 22. (a) Comparison of *D-Viewer* and the sensor; (b) result of all measuring points by *D-Viewer*

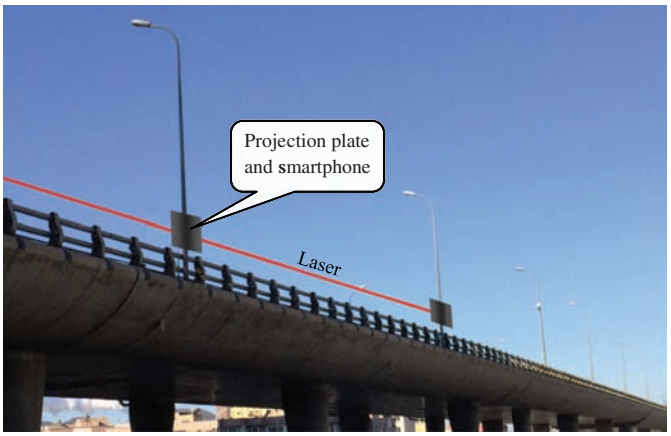

Fig. 24. (Color) Schematic of device installation (image by Qingan Zhao)

can be applied to real bridge structures. Several ideas are given to promote future research.

First, device installation must be considered. Because most long-span bridges and many short-span bridges have light poles or utility poles, it is possible to install the laser transmitter and projection plate on those poles where people are able to place their smartphones into the appropriate position, as shown in Fig. 24. Because poles are always located on the border of roads and sidewalks or on the edge of the bridge, the laser is unlikely to be blocked by pedestrians or vehicles. Installations should be designed to be detachable for device maintenance and improvement. Devices could also be installed on railings or temporary fixed supports if the poles are not appropriate for installation or if there are no poles on the bridge.

Many challenges can be encountered when implementing monitoring on real bridge structures. Distributed displacement monitoring needs time synchronization. Because push notifications are not able to reach all smartphones at exactly the same time, smartphones should have unified clocks and should save the acquisition time in data files. As for noise, such as ambient vibration in the process of monitoring, signal analysis techniques have long been used for denoise processing in bridge SHM, such as filtering (Deraemaeker et al. 2008) and wavelet transform (Donoho and Johnstone 1994). Moschas and Stiros (2011) developed a multistep filtering procedure and managed to denoise GPS recordings of the dynamic displacement of a bridge. They used GPS receivers at a 10-Hz sampling rate, so it is possible to utilize this procedure and attain even better performance using 30-Hz sampling-rate smartphone receivers. Another challenge is range, so at present the technique mainly focuses on short-span and medium-span bridges. For future research on long-range applications, although lasers cannot transmit long distances without dispersing, laser transmitters can transfer measurements one by one without transmitting over a long distance. Angle change due to rotation of a structure at the installation location may cause huge errors when transferring measurements,

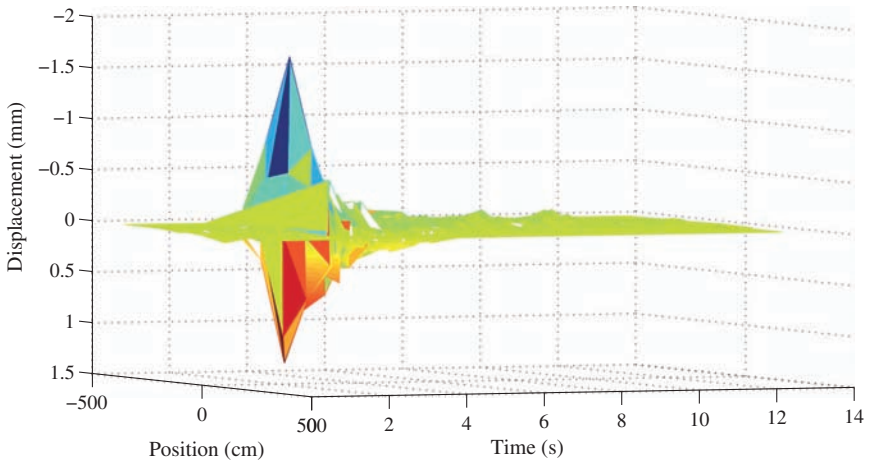

Fig. 23. (Color) Real-time deformation graph of the impact

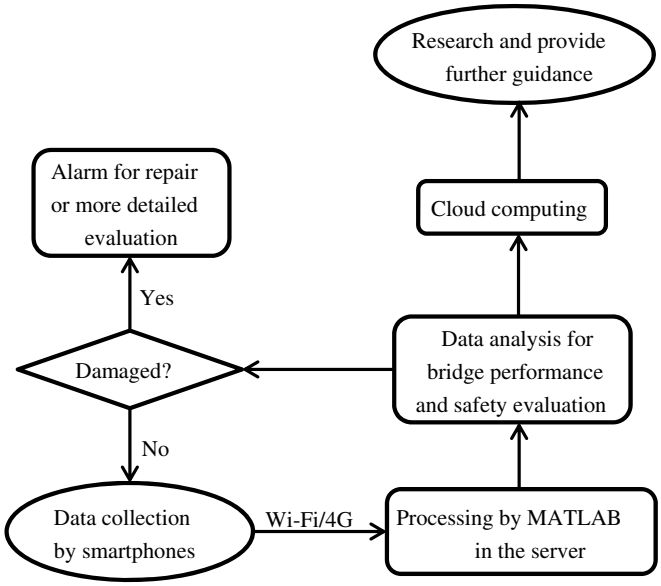

Fig. 25. Displacement monitoring system

but it is likely to be eliminated by the displacement error back-propagation method proposed by Jeon et al. (2012).

Furthermore, a preliminary idea for a displacement monitoring system based on this technique is proposed, as shown in Fig. 25. It consists of two main components, a monitoring part and a cloud-computing part. First, displacement data can be collected by smartphones. Through a connection by Wi-Fi or 4G, all data can be uploaded to servers. Algorithms designed for data analysis in the servers evaluate the performance and safety of the bridges. If damage is detected, messages are sent to the bridge maintenance department alerting them to the need for repair or more detailed evaluation. Meanwhile, analyzed data are also uploaded for cloud computing, which aims to provide more guidance for bridge maintenance and management.

Conclusions

This paper proposes a distributed bridge displacement monitoring and inspection technique using an app and a laser projector. By attaching a laser pointer and projecting the beam onto a plate, the camera sensor in the smartphone can monitor the movement of the structure by observing the laser spot. A series of experiments, including static and dynamic experiments, was implemented to evaluate this method. The following conclusions can be drawn:

- There are far-reaching prospects in this economical, convenient, and efficient technique, which will serve as a complement to conventional SHM techniques;
- Due to the good operability of *D-Viewer* and the popularity of smartphones, almost anyone can participate in displacement investigations with simple instruction;
- This technique is accurate and stable enough for displacement monitoring and inspection. There is good agreement between the monitored data and data from traditional displacement sensor;
- With data processing, this technique can be used for preliminary analysis of the performance of the structure;
- Application of this technique to real bridges is discussed, and possible solutions are purposed to overcome the challenges; and
- This technique is not limited to monitoring and inspecting the displacement of bridges. It can be extended to other infrastructures.

To promote this technique to provide better service and to allow it to be widely used, *D-Viewer* has been uploaded to the App Store and can be downloaded for free.

Acknowledgments

The authors acknowledge the financial supports of National Natural Science Foundation of China (51278085, 51221961).

Conflicts of Interest

The authors declare no conflict of interest.

References

Apple Inc. (2016). "Tech specs." ⟨http://www.apple.com/iphone-6/specs/⟩ (May 1, 2016).

Backer, H. D., Outtier, A., and Bogaert, P. V. (2014). "Determining geometric out-of-plane imperfections in steel tied-arch bridges using strain measurements." *J. Perform. Constr. Facil.*, 10.1061/(ASCE)CF.1943-5509.0000445, 549–558.

Balageas, D., Fritzen, C. P., and Güemes, A. (2010). "Introduction to structural health monitoring." *Structural health monitoring*, ISTE, Arlington, TX.

Brownjohn, J. M. W. (2007). "Structural health monitoring of civil infrastructure." *Philos. Trans. R. Soc. Ser. A Math. Phys. Eng. Sci.*, 365(1851), 589–622.

Deraemaeker, A., Reynders, E., Roeck, G. D., and Kullaa, J. (2008). "Vibration-based structural health monitoring using output-only measurements under changing environment." *Mech. Syst. Signal Process.*, 22(1), 34–56.

Donoho, D. L., and Johnstone, J. M. (1994). "Ideal spatial adaptation by wavelet shrinkage." *Biometrika*, 81(3), 425–455.

Feng, M., Fukuda, Y., Mizuta, M., and Ozer, E. (2015). "Citizen sensors for SHM: Use of accelerometer data from smartphones." *Sensors*, 15(2), 2980–2998.

Fumagalli, I. E. (1973). "Principles of similitude." *Statical and geomechanical models*, Springer, Vienna.

Han, R., Zhao, X., Yan, Y., Guan, Q., Hu, W., and Li, M. (2016). "A cyber-physical system for girder hoisting monitoring based on smartphones." *Sensors*, 16(7), 1048.

Höpfner, H., Morgenthal, G., Schirmer, M., Naujoks, M., and Halang, C. (2013). "On measuring mechanical oscillations using smartphone sensors: Possibilities and limitation." *ACM SIGMOBILE Mobile Comput. Commun. Rev.*, 17(4), 29–41.

Housner, G. W., Bergman, L. A., Caughey, T. K., Chassiakos, A. G., Claus, R. O., and Masri, S. F. (1997). "Special issue, structural control: Past, present and future." *J. Eng. Mech.*, 10.1061/(ASCE)0733-9399(1997)123:9(897), 897–971.

Iwao, M., Ryuta, K., Maya, S., Miroku, I., Hideaki, K., and Kiyoshi, K. (2010). "Measuring relative-story displacement and local inclination angle using multiple position-sensitive detectors." *Sensors*, 10(11), 9687–9697.

Jeon, H., Shin, J. U., Myeong, W., and Myung, H. (2012). "Multiple ViSPs (visually servoed paired structured light systems) for 6-DOF structural displacement estimation." *Int. Conf. on Ubiquitous Robots and Ambient Intelligence*, IEEE, New York, 167–169.

Kwasniewski, L., Wekezer, J., Roufa, G., Li, H., Ducher, J., and Malachowski, J. (2006). "Experimental evaluation of dynamic effects for a selected highway bridge." *J. Perform. Constr. Facil.*, 10.1061/(ASCE)0887-3828(2006)20:3(253), 253–260.

Lee, J. J., and Shinozuka, M. (2006). "Real-time displacement measurement of a flexible bridge using digital image processing techniques." *Exp. Mech.*, 46(1), 105–114.

Mazen Wahbeh, A., Caffrey, J. P., and Masri, S. F. (2003). "A vision-based approach for the direct measurement of displacements in vibrating systems." *Smart Mater. Struct.*, 12(5), 785–794.

Moschas, F., and Stiros, S. (2011). "Measurement of the dynamic displacements and of the modal frequencies of a short-span pedestrian bridge using GPS and an accelerometer." *Eng. Struct.*, 33(1), 10–17.

Oraczewski, T., Staszewski, W. J., and Uhl, T. (2016). "Nonlinear acoustics for structural health monitoring using mobile, wireless and smartphone-based transducer platform." *J. Intell. Mater. Syst. Struct.*, 27(6), 786–796.

Ou, J. (2005). "Some recent advances of intelligent health monitoring systems for civil infrastructures in HIT." *Fundamental Problems of Optoelectronics and Microelectronics II*, SPIE, Bellingham, WA.

Ozcan, A. (2014). "Mobile phones democratize and cultivate next-generation imaging, diagnostics and measurement tools." *Lab Chip*, 14(17), 3187–3194.

Ozer, E., Feng, M. Q., and Feng, D. (2015). "Citizen sensors for SHM: Towards a crowdsourcing platform." *Sensors*, 15(6), 14591–14614.

Reilly, J., Dashti, S., Ervasti, M., Bray, J. D., Glaser, S. D., and Bayen, A. M. (2013). "Mobile phones as seismologic sensors: Automating data extraction for the iShake system." *IEEE Trans. Autom. Sci. Eng.*, 10(2), 242–251.

Sangho, B. (2001). "The component development of digital close range photogrammetry for the construction structure displacement analysis." *New Technology for a New Century Int. Conf.*, FIG Working Week, Seoul.

Statista Inc. (2016). "Smartphone users worldwide." ⟨https://www.statista.com/statistics/330695/number-of-smartphone-users-worldwide/⟩ (Oct. 20, 2016).

Wang, Y. L., Liu, X. L., and Fang, C. Q. (2012). "Damage detection of bridges by using displacement data of two symmetrical points." *J. Perform. Constr. Facil.*, 10.1061/(ASCE)CF.1943-5509.0000240, 300–311.

Yi, W. J., Gilliland, S., and Saniie, J. (2013). "Wireless sensor network for structural health monitoring using system-on-chip with android smartphone." *2013 IEEE Sensors*, Baltimore, 1–4.

Yi, W. J., Jia, W., and Saniie, J. (2012). "Mobile sensor data collector using android smartphone." *Midwest Symp. on Circuits and Systems*, IEEE, New York, 956–959.

Yu, Y., et al. (2015). "Initial validation of mobile-structural health monitoring method using smartphones." *Int. J. Distrib. Sens. Netw.*, 111(2), 1–14.

Yu, Y., Zhao, X., and Ou, J. (2012). "A new idea: Mobile structural health monitoring using smart phones." *Int. Conf. on Intelligent Control and Information Proc.*, 714–716.

Zhao, X., et al. (2015a). "Bridge displacement monitoring method based on laser projection-sensing technology." *Sensors*, 15(4), 8444–8463.

Zhao, X., et al. (2015b). "Portable and convenient cable force measurement using smartphone." *J. Civ. Struct. Health Monit.*, 5(4), 481–491.

Zhao, X., Liu, H., Yu, Y., Zhu, Q., Hu, W., and Li, M. (2016). "Displacement monitoring technique using a smartphone based on the laser projection-sensing method." *Sens. Actuators A*, 246, 35–47.

Zhao, X., Yu, Y., Li, M. C., and Ou, J. P. (2015c). "Cloud-structural health monitoring based on smartphone." *Int. Conf. on Vibroengineering in Nanjing*, Vibroengineering Procedia, Kaunas, Lithuania.